Zou, Yuanmin; Chernyaev, Alexander; Seisko, Sipi; Sainio, Jani; Lundström, Mari

# Removal of iron and aluminum from hydrometallurgical NMC-LFP recycling process through precipitation

*Published in:*
Minerals Engineering

*DOI:*
10.1016/j.mineng.2024.109037

Published: 01/11/2024

*Document Version*
Publisher's PDF, also known as Version of record

Minerals Engineering 218 (2024) 109037

Contents lists available at ScienceDirect

Minerals Engineering

journal homepage: www.elsevier.com/locate/mineng

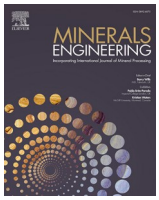

# Removal of iron and aluminum from hydrometallurgical NMC-LFP recycling process through precipitation

Yuanmin Zou [a], Alexander Chernyaev [a,b], Sipi Seisko [a], Jani Sainio [c], Mari Lundström [a,*]

[a] Department of Chemical and Metallurgical Engineering, School of Chemical Engineering, Aalto University, 00076 Aalto, Finland
[b] Metso Outotec Research Center, Kuparitie 10, 28101 Pori, Finland
[c] Department of Applied Physics, School of Science, Aalto University, 00076 Aalto, Finland

ARTICLE INFO

*Keywords:*
Black mass
Lithium-ion battery
Cathode active material
Fluorine removal
Copper
Phosphate

ABSTRACT

There is a need to develop removal strategies for typical battery impurities–iron and aluminum–from actual hydrometallurgical recycling solutions. In this work, the investigated solution originated from lithium nickel manganese cobalt oxide (NMC) rich black mass, while iron phosphate (LFP) was used as an in situ reductant. It was found that the presence of phosphate ions supported selective iron precipitation already at pH = 2.0 ($T$ = 60 °C, $t$ = 3 h, NaOH), with nearly complete iron removal (97.8 %). The precipitate was rich in iron (21.5 wt%) and phosphorus (13.4 wt%); it also contained 0.7 wt% Ni and 0.3–0.4 wt% Mn, Co, Al, and Li. It is suggested that the presence of phosphate in minor amounts may cause this co-precipitation of battery metals. With the aim of combined precipitation of iron (100 %) and aluminum (91.0 %), the pH was increased up to 4.5. Although 90.8 % of fluoride precipitated, the remaining fluorides may have kept the aluminum partially in soluble form as Al-F complexes. The formed precipitate had lower iron (18.4 wt%) and phosphorus (11.4 wt%) content, whereas the impurity contents and thus the battery metals losses were slightly higher: Ni, Mn, Co, Al, and Cu were each between 1.1–1.9 wt% and Li and F < 1 wt%. In the precipitates investigated, iron was found predominantly as iron phosphate ($FePO_4$), whereas a minor fraction also precipitated as iron fluoride ($FeF_3$). The precipitated aluminum existed mainly as AlOOH. The results presented here will help to build iron and aluminum removal strategies for industrial battery recycling solutions, and also provide insights into the dominant iron and aluminum phases forming the precipitates.

## 1. Introduction

The process of metal recovery from spent lithium-ion batteries (LIBs) involves multiple unit processes focused on recycling and reclaiming valuable materials. Generally, LIBs collected from diverse sources are first discharged and sorted mechanically, dismantled from their casings, and subsequently broken down into smaller components like cells, or crushed, either manually or through automated processes (Guan et al., 2017; Shin et al., 2005; Song et al., 2017). The small particle size fraction concentrated with active materials (cathode and anode) is referred to as black mass (BM). Valuable metals (such as Co and Ni) can be extracted from BM either via hydrometallurgical processes (Chen and Ho, 2018; Guzolu et al., 2017; Partinen et al., 2022; Takacova et al., 2016; Yuliusman et al., 2018) or pyro-hydrometallurgical processes. In pyrometallurgical treatment (Lombardo et al., 2019; Makuza et al., 2021), the target metals are transformed into alloy (smelting), oxides (calcination) (Hu et al., 2013), or easily leachable components (roasting) (Paulino et al., 2008), whereas lithium may be fumed (Scheunis and Callebaut, 2023) or retained in the slag for further extraction (Sun et al., 2017) or disposal. During hydrometallurgical processing, leaching, separation, and purification techniques are then employed for the refining of pure battery metals and/or salts. Current practices have demonstrated the effective recovery of Ni, Co, and Cu from BM (European Commission, 2023), and industrial large-scale recycling plants are currently exploring the recovery of Li, Mn, and graphite (Rinne et al., 2021). In contrast, elements like F, Fe, and Al are viewed as impurities in LIB recycling processes due to their low value and the negative impacts they have on the recovery of other elements.

The recently published European Battery regulation (European Commission, 2023) demands both higher recovery efficiency of total mass as well as of individual elements; however, no element–specific requirements exist for Fe, Al, or P, and they are still considered as

* Corresponding author.
*E-mail address:* mari.lundstrom@aalto.fi (M. Lundström).

https://doi.org/10.1016/j.mineng.2024.109037
Received 12 July 2024; Received in revised form 27 September 2024; Accepted 28 September 2024
Available online 2 October 2024

**Table 1**
Equilibrium reactions, constants, and chemical equilibrium constants equations for $Fe^{2+}$/ $Fe^{3+}$-$Al^{3+}$-$SO_4^{2-}$-$PO_4^{3-}$-$F^-$–$H_2O$ system at 25 °C.

| No. | Equilibrium reactions | Constants | Chemical equilibrium constants equations |
|---|---|---|---|
| (1) | $H_2O \rightleftharpoons H^+ + OH^-$ | $10^{-14}$ | $10^{-14} = [H^+][OH^-]$ |
| (2) | $H_2SO_4 \rightleftharpoons H^+ + HSO_4^-$ | $10^{3}$ | $10^{-3} = [HSO_4^-][H^+]/[H_2SO_4]$ |
| (3) | $HSO_4^- \rightleftharpoons H^+ + SO_4^{2-}$ | $10^{-1.99}$ | $10^{-1.99} = [SO_4^{2-}][H^+]/[HSO_4^-]$ |
| (4) | $H^+ + PO_4^{3-} \rightleftharpoons HPO_4^{2-}$ | $10^{12.36}$ | $10^{12.36} = [HPO_4^{2-}]/\{[PO_4^{3-}][H^+]\}$ |
| (5) | $H^+ + HPO_4^{2-} \rightleftharpoons H_2PO_4^-$ | $10^{7.20}$ | $10^{7.20} = [H_2PO_4^-]/\{[HPO_4^{2-}][H^+]\}$ |
| (6) | $H^+ + H_2PO_4^- \rightleftharpoons H_3PO_4$ | $10^{2.15}$ | $10^{2.15} = [H_3PO_4]/\{[H^+]/[HPO_4^{2-}]$ |
| (7) | $Fe^{3+} + OH^- \rightleftharpoons Fe(OH)^{2+}$ | $10^{11.87}$ | $10^{11.87} = [Fe(OH)^{2+}]/\{[OH^-][Fe^{3+}]\}$ |
| (8) | $Fe^{3+} + 2OH^- \rightleftharpoons Fe(OH)_2^+$ | $10^{21.17}$ | $10^{21.17} = [Fe(OH)^{2+}]/\{[OH^-]^2\ [Fe^{3+}]\}$ |
| (9) | $Fe^{3+} + 3OH^- \rightleftharpoons Fe(OH)_{3(aq)}$ | $10^{29.67}$ | $10^{29.67} = [Fe(OH)_{3(aq)}]/\{[OH^-]^3\ [Fe^{3+}]\}$ |
| (10) | $Fe^{3+} + 4OH^- \rightleftharpoons Fe(OH)_4^-$ | $10^{34.4}$ | $10^{34.4} = [Fe(OH)_4]/\{[OH^-]^4\ [Fe^{3+}]\}$ |
| (11) | $2Fe^{3+} + 2OH^- \rightleftharpoons Fe_2(OH)_2^{4+}$ | $10^{25.1}$ | $10^{25.1} = [Fe_2(OH)_2^{4+}]/\{[OH^-]^2\ [Fe^{3+}]^2\}$ |
| (12) | $3Fe^{3+} + 4OH^- \rightleftharpoons Fe_3(OH)_4^{5+}$ | $10^{49.7}$ | $10^{49.7} = [Fe_3(OH)_4^{5+}]/\{[OH^-]^4\ [Fe^{3+}]^3\}$ |
| (13) | $Fe^{3+} + SO_4^{2-} \rightleftharpoons FeSO_4^+$ | $10^{2.03}$ | $10^{2.03} = [FeSO_4^+]/\{[SO_4^{2-}][Fe^{3+}]\}$ |
| (14) | $Fe^{3+} + 2SO_4^{2-} \rightleftharpoons Fe(SO_4)_2^-$ | $10^{2.98}$ | $10^{2.98} = [Fe(SO_4)_2]/\{[SO_4^{2-}]^2\ [Fe^{3+}]\}$ |
| (15) | $Fe^{3+} + HPO_4^{2-} \rightleftharpoons FeHPO_4^+$ | $10^{8.30}$ | $10^{8.30} = [FeHPO_4^+]/\{[HPO_4^{2-}][Fe^{3+}]\}$ |
| (16) | $Fe^{3+} + H_2PO_4^- \rightleftharpoons FeH_2PO_4^{2+}$ | $10^{3.47}$ | $10^{3.47} = [FeH_2PO_4^{2+}]/\{[H_2PO_4^-]\ [Fe^{3+}]\}$ |
| (17) | $Fe^{3+} + F^- \rightleftharpoons FeF^{2+}$ | $10^{5.28}$ | $10^{5.28} = [FeF^{2+}]/\{[F^-][Fe^{3+}]\}$ |
| (18) | $Fe^{3+} + 2F^- \rightleftharpoons FeF_2^+$ | $10^{9.30}$ | $10^{9.30} = [\ FeF_2^+]/\{[F^-]^2[Fe^{3+}]\}$ |
| (19) | $Fe^{3+} + 3F^- \rightleftharpoons FeF_{3(aq)}$ | $10^{12.06}$ | $10^{12.06} = [FeF_{3(aq)}]/\{[F^-]^3\ [Fe^{3+}]\}$ |
| (20) | $Fe^{2+} + OH^- \rightleftharpoons Fe(OH)^+$ | $10^{5.56}$ | $10^{5.56} = [Fe(OH)^+]/\{[OH^-][Fe^{2+}]\}$ |
| (21) | $Fe^{2+} + 2OH^- \rightleftharpoons Fe(OH)_{2(aq)}$ | $10^{9.77}$ | $10^{9.77} = [Fe(OH)_{2(aq)}]/\{[OH^-]^2\ [Fe^{2+}]\}$ |
| (22) | $Fe^{2+} + 3OH^- \rightleftharpoons Fe(OH)_3^-$ | $10^{9.67}$ | $10^{9.67} = [Fe(OH)^-]/\{[OH^-]^3\ [Fe^{2+}]\}$ |
| (23) | $Fe^{2+} + 4OH^- \rightleftharpoons Fe(OH)_4^{2-}$ | $10^{8.58}$ | $10^{8.58} = [Fe(OH)_4^{2-}]/\{[OH^-]^4\ [Fe^{2+}]\}$ |
| (24) | $Fe^{2+} + SO_4^{2-} \rightleftharpoons FeSO_{4(aq)}$ | $10^{2.2}$ | $10^{2.2} = [FeSO_{4(aq)}]/\{[SO_4^{2-}]\ [Fe^{2+}]\}$ |
| (25) | $Fe^{2+} + HPO_4^{2-} \rightleftharpoons FeHPO_{4(aq)}$ | $10^{3.6}$ | $10^{3.6} = [FeHPO_{4(aq)}]/\{[HPO_4^{2-}][Fe^{2+}]\}$ |
| (26) | $Fe^{2+} + H_2PO_4^- \rightleftharpoons FeH_2PO_4^+$ | $10^{2.7}$ | $10^{2.7} = [FeH_2PO_4^+]/\{[H_2PO_4^-][Fe^{2+}]\}$ |
| (27) | $Fe^{2+} + F^- \rightleftharpoons FeF^+$ | $10^{9.07}$ | $10^{9.07} = [FeF^+]/\{[F^-][Fe^{2+}]\}$ |
| (28) | $Al^{3+} + OH^- \rightleftharpoons Al(OH)^{2+}$ | $10^{9.27}$ | $10^{9.27} = [Al(OH)^{2+}]/\{[OH^-][Al^{3+}]\}$ |
| (29) | $Al^{3+} + 2OH^- \rightleftharpoons Al(OH)_2^+$ | $10^{18.7}$ | $10^{18.7} = [Al(OH)^{2+}]/\{[OH^-]^2\ [Al^{3+}]\}$ |
| (30) | $Al^{3+} + 3OH^- \rightleftharpoons Al(OH)_{3(aq)}$ | $10^{27}$ | $10^{27} = [Al(OH)_{3(aq)}]/\{[OH^-]^3\ [Al^{3+}]\}$ |
| (31) | $Al^{3+} + 4OH^- \rightleftharpoons Al(OH)_4^-$ | $10^{33.03}$ | $10^{33.03} = [Al(OH)_4^-]/\{[OH^-]^4[Al^{3+}]\}$ |
| (32) | $2Al^{3+} + 2OH^- \rightleftharpoons Al_2(OH)_2^{4+}$ | $10^{20.3}$ | $10^{20.3} = [Al_2(OH)_2^{4+}]/\{[OH^-]^2\ [Al^{3+}]^2\}$ |
| (33) | $3Al^{3+} + 4OH^- \rightleftharpoons Al_3(OH)_4^{5+}$ | $10^{42.1}$ | $10^{42.1} = [Al_3(OH)_4^{5+}]/\{[OH^-]^4\ [Al^{3+}]^3\}$ |
| (34) | $Al^{3+} + F^- \rightleftharpoons AlF^{2+}$ | $10^{6.10}$ | $10^{6.10} = [AlF^{2+}]/\{[F^-][Al^{3+}]\}$ |
| (35) | $Al^{3+} + 2F^- \rightleftharpoons AlF_2^+$ | $10^{11.15}$ | $10^{11.15} = [AlF_2^+]/\{[F^-]^2[Al^{3+}]\}$ |
| (36) | $Al^{3+} + 3F^- \rightleftharpoons AlF_{3(aq)}$ | $10^{15.00}$ | $10^{15.00} = [AlF_{3(aq)}]/\{[F^-]^3\ [Al^{3+}]\}$ |
| (37) | $Al^{3+} + 4F^- \rightleftharpoons AlF_4^-$ | $10^{17.75}$ | $10^{17.75} = [AlF_4^-]/\{[F^-]^4[Al^{3+}]\}$ |
| (38) | $Al^{3+} + 5F^- \rightleftharpoons AlF_5^{2-}$ | $10^{19.37}$ | $10^{19.37} = [AlF_5^{2-}]/\{[F^-]^5\ [Al^{3+}]\}$ |
| (39) | $Al^{3+} + 6F^- \rightleftharpoons AlF_6^{3-}$ | $10^{19.84}$ | $10^{19.84} = [AlF_6^{3-}]/\{[F^-]^6\ [Al^{3+}]\}$ |
| (40) | $Fe(OH)_{3(s)} \rightleftharpoons Fe^{3+} + 3OH^-$ | $10^{-38.55}$ | $10^{-38.55} = [OH^-]^3\ [Fe^{3+}]$ |
| (41) | $FePO_{4(s)} \rightleftharpoons Fe^{3+} + PO_4^{3-}$ | $10^{-21.89}$ | $10^{-21.89} = [PO_4^{3-}]\ [Fe^{3+}]$ |
| (42) | $FePO_4{\cdot}2H_2O_{(s)} \rightleftharpoons Fe^{3+} + PO_4^{3-} + 2H_2O$ | $10^{-15.00}$ | $10^{-15.00} = [PO_4^{3-}]\ [Fe^{3+}]$ |
| (43) | $FeF_{3(s)} \rightleftharpoons Fe^{3+} + 3F^-$ | $10^{-24.44}$ | $10^{-24.44} = [F^-]^3\ [Fe^{3+}]$ |
| (44) | $Fe(OH)_{2(s)} \rightleftharpoons Fe^{2+} + 2OH^-$ | $10^{-16.31}$ | $10^{-16.31} = [OH^-]^2\ [Fe^{2+}]$ |
| (45) | $FeF_{2(s)} \rightleftharpoons Fe^{2+} + 2F^-$ | $10^{-5.63}$ | $10^{-5.63} = [F^-]^2\ [Fe^{2+}]$ |
| (46) | $Fe_3(PO_4)_2{\cdot}8H_2O_{(s)} \rightleftharpoons 3Fe^{2+} + 2PO_4^{3-} + 8H_2O$ | $10^{-36.85}$ | $10^{-36.85} = [PO_4^{3-}]^2\ [Fe^{2+}]^3$ |
| (47) | $Al(OH)_{3(s)} \rightleftharpoons Al^{3+} + 3OH^-$ | $10^{-32.89}$ | $10^{-32.89} = [OH^-]^3\ [Al^{3+}]$ |
| (48) | $AlPO_{4\ (s)} \rightleftharpoons Al^{3+} + PO_4^{3-}$ | $10^{-20.01}$ | $10^{-20.01} = [PO_4^{3-}]\ [Al^{3+}]$ |
| (50) | $AlF_{3(s)} \rightleftharpoons Al^{3+} + 3F^-$ | $10^{-16.34}$ | $10^{-16.34} = [F^-]^3\ [Al^{3+}]$ |

impurities. Thus, conventionally, the main target in their recovery can be stated to be the minimization of valuable metals losses (Co, Ni, Cu, Li) in their removal while producing environmentally stable waste with minimized processing costs. In the future, more ambitious goals for Al, Fe, or P valorization may appear for these currently overlooked elements. This is further highlighted by the fact that Al can pose an environmental burden if subjected to the linear economy (Rinne et al., 2021) and P has been listed as a strategic raw material for the EU since 2017 (European Commission, 2017), essential for industrial and agricultural purposes (Daneshgar et al., 2018). P is primarily sourced from phosphate rock, a resource characterized by its finite, irreplaceable, and nonrenewable nature (Cordell et al., 2009; Daneshgar et al., 2018), with current reserves expected to be depleted within 100 to 250 years (Johnston and Steen, 2002). The demand for P is predicted to increase by 50–100 % by 2025 (Cordell et al., 2009). This further encourages moving the focus to phosphorus recovery from battery waste.

In LIB leaching, BM metals, such as Li, Co, Ni, Mn, Cu, Fe, and Al, are mostly dissolved in mineral acids (Lv et al., 2018; Velázquez-Martínez et al., 2019). The pregnant leaching solution (PLS) compositions have been reported to vary, depending on the raw materials and conditions used in the process: 5.4–27.4 g/L Co, 2–12.7 g/L Ni, 1.3–5.8 g/L Mn, 1.2–3.8 g/L Li, 0.05–3.7 g/L Cu, 1.0–2.9 g/L Al, and 0.02–1.3 g/L Fe (Jantunen et al., 2022; Peng et al., 2020; Porvali et al., 2019; Wesselborg et al., 2021; Zhang et al., 2022). Currently, battery waste already has higher Ni content (Agarwal et al., 2019), and P and Fe contents are likely to increase in the near future (Jie et al., 2021) if LFP battery waste is integrated into state-of-the-art processing. It has previously been shown that the synergistic use of LFP waste can promote the reductive power of leaching (Jiang et al., 2021; Zou et al., 2024); however, the mass and energy balance feasibility of holistic processing should be considered. From the point of view of synergistic processing, LFP also adds elements such as lithium ions ($Li^+$), ferrous ions ($Fe^{2+}$), and phosphate ions ($PO_4^{3-}$) to the solution. $PO_4^{3-}$ can change the anion composition of the PLS but is also capable of forming soluble and solid compounds that increase the variety of species present in the solution. It is known that aluminum and iron can form precipitates such as aluminum phosphate ($AlPO_4$), $FePO_4$, and ferrous iron phosphate ($Fe_3(PO_4)_2{\cdot}8H_2O$) with solubility product constant (*Ksp*) values of $9.84\times10^{-21}$, $1.30\times10^{-22}$, and $1.41\times10^{-37}$, respectively, at 25 °C. Additionally, they compete with anions to form complexes, Table 1(Jie et al., 2021; Kotrlý and Šůcha, 1985; Martell and

Smith, 1976; Speight and Lang, 2004).

If not removed, impurities can be harmful to downstream separation processes, as well as impacting the functionality of the final products. These impurities effectively compete with the main metal elements during the processes of solvent extraction (SX) (Pranolo et al., 2010; Zhang et al., 2022), ion exchange (IX) (Virolainen et al., 2021), and chemical precipitation (Kang et al., 2010), thus reducing the overall yield of targeted metals like Ni and Co in recovery processes. Therefore, it is especially important to recover these impurity elements during the spent LIB recycling process. Furthermore, all LIB waste materials contain fluorides, which have been largely overlooked in the existing studies of Fe and Al removal (Jie et al., 2021; Klaehn et al., 2023). Fluorine (F) can form soluble complexes, generating $FeF^{2+}$ and/or $FeF_2^+$ with Fe as well as $AlF^{2+}$, $AlF_2^+$, $AlF_3$(aq), $AlF_4^-$, $AlF_5^{2-}$, and $AlF_6^{3-}$ with Al (Table 1). These fluoride solution species can also potentially interfere with the precipitation of Fe and Al.

Although acid is consumed during BM leaching, the aim of the low pH value is to keep all metals in a dissolved state (i.e., avoiding uncontrolled hydrolysis of Fe, Al, Cu, Co, Ni, etc.). Therefore, the pH of the PLS is typically kept below 2. Solution purification of PLS includes a controlled rise in pH in order to first remove impurities such as Al and Fe. Consequently, the PLS pH is then further raised to support the recovery of the target battery metals, e.g., the extraction of Mn, Co, and Ni via SX occurs typically at a pH range of 3.5–5.0 with phosphorus extractants (Dobó et al., 2023).

This work focuses on Al and Fe removal from PLS that consists of dissolved industrial NMC waste in the presence of LFP at pH values of 2.0–4.5. The goal was to investigate the role of $PO_4^{3-}$ ions in the Al and Fe removal step of the solution purification process, specifically under conditions where $Cu^{2+}$ ions are also dissolved, as well as $F^-$ ions being present. The results contribute to increased understanding of separation efficiency, precipitates, and product purities via a precipitation method in complex industrial processes involving NMC and LFP waste recycling, thereby providing valuable information for the separation techniques used in hydrometallurgical applications.

## 2. Experimental

### 2.1. Raw materials

The PLS used as the raw material originated from leaching tests conducted for industrial NMC BM (50 g) using synthetic LFP (particle size D50: 1.5 μm, MSE Supplies) as a reductant (28.3 g) at 1.5 M $H_2SO_4$ ($T = 60$ °C, $S/L = 156$ g/L, $t = 3$ h). The detailed leaching procedure is presented in our previous published work (Zou et al., 2024). Industrial NMC BM consisted of 15.8 wt% Ni, 8.4 wt% Mn, 8.7 wt% Co, 4.1 wt% Li, 9.8 wt% P, 0.1 wt% Fe, 2.3 wt% Cu, 2.4 wt% Al, and 1.0 wt% F. Three repeated leaching tests were conducted to produce the PLS ($V_{TOT} = 1245$ mL). The chemical composition of the PLS was analyzed using atomic absorption spectroscopy (AAS, Thermo Fisher ICE 3000) operated with an air-acetylene flame. Al and P were measured using inductively coupled plasma-optical emission spectrometry (ICP-OES, Agilent 5900 SVDV). Additionally, the determination of fluorine content was carried out using the I-F-ISE method (ALS Oy, Helsinki). The pH was adjusted with 1.0 M $H_2SO_4$ and 2.5 M NaOH, of which the 1.0 M $H_2SO_4$ was prepared from technical grade sulfuric acid (Sigma Aldrich, VWR Chemicals, 95 %) and the 2.5 M NaOH from reagent grade sodium hydroxide (Sigma Aldrich, powder, ≥ 97 %) and distilled water. The accuracy of the concentration for 1 M acid was verified through titration, using a standardized 0.2 M NaOH solution (Merck, Titripur). Table 2 shows the elemental composition of the studied PLS ($[H_2SO_4] = 0.224$ M).

### 2.2. Precipitation for Al and Fe removal

Precipitation tests were conducted on PLS solution samples ($V = 60$ mL) at $T = 60$ °C for 3 h. The predetermined target pH values in the experiments varied in the range of 2.0 to 4.5, Table 3. Each experiment was carried out in a beaker with a jacketed system and 300 rpm agitation, and repeated three times. Solutions of 2.5 M NaOH and 1 M $H_2SO_4$ were used to adjust the solution to reach the target pH value, both of which were added dropwise via a 25 ml glass burette. An online pH meter (METTLER TOLEDO Seven Compact™ S210) was used throughout the experiment. After the target pH was reached, the test was initiated and continued for 3 h. The pH value was adjusted every 20 min during the first hour and every 30 min in the following two hours.

When the precipitation was completed, S/L separation was conducted by vacuum filtration with Whatman 41 filter paper (diameter: 90 mm) and a Buchner funnel. Solutions were collected and the precipitates were washed with acidified water corresponding to the experimental pH value. The washing solution was measured and analyzed for metal concentrations. The cakes were dried for 72 h at room temperature (using a fume hood) and the total weight measured. Approximately 0.5 g of each cake was digested with 4 ml of 37 % HCl at 60 °C (in a volumetric flask) and the cooled solution analyzed by AAS and ICP (Al and P). The fluorine amount in the liquid samples, including filter solution, wash water, and dissolved cake, was analyzed. The co-precipitated metal content (Ni, Co, Mn, Li, and Cu) in the cake was calculated using Eq. (51):

$$E(\%) = \left( \frac{c_{cake}^{Me} \times m_{tot}^{cake}}{c_i^{Me} \times V_i^{sol}} \right) \times 100, \quad (51)$$

where $c_{cake}^{Me}$ is the metal content in the cake (g/kg), $m_{tot}^{cake}$ is the total mass of the cake (kg), $c_i^{Me}$ is the initial metal concentration in the leach solution (g/L), and $V_i^{sol}$ is the volume of the starting leach solution (L). The iron, phosphorus, and aluminum extraction were calculated using Eq. (52):

$$E(\%) = 100 - \left( \frac{(c_f \times V_f) + (c_{ww} \times V_{ww})}{(c_i^{Me} \times V_i^{sol})} \times 100 \right), \quad (52)$$

where $c_f$ is the concentration of metal in the final solution (g/L), $V_f$ is the final volume of the solution (L), $c_{ww}$ is the concentration of metal in wash water (g/L), and $V_{ww}$ is the final volume of the wash water (L).

The phase compositions of the precipitates were studied using an X-ray diffraction device (XRD, Pro MPD Powder, USA) equipped with a PIXcel1D detector and a Cu Kα source. The XRD device was operated at

**Table 3**
Experimental precipitation series for PLS ($t = 3$ h, $T = 60$ °C, $\omega = 300$ rpm).

| Experiment | pH value |
|---|---|
| P1-1#, P1-2#, P1-3# | 2.0 |
| P2-1#, P2-2#, P2-3# | 2.5 |
| P3-1#, P3-2#, P3-3# | 3.0 |
| P4-1#, P4-2#, P4-3# | 3.5 |
| P5-1#, P5-2#, P5-3# | 4.0 |
| P6-1#, P6-2#, P6-3# | 4.5 |

**Table 2**
Composition of the PLS ($pH = 0.95$) used in the study.

| Mix PLS | Ni | Mn | Co | Li | P | Fe | Cu | Al | F |
|---|---|---|---|---|---|---|---|---|---|
| Concentration (g/L) | 12.72 | 6.96 | 7.51 | 5.90 | 11.06 | 18.04 | 2.09 | 1.19 | 1.41 |

40 kV and 40 mA, utilizing an Fe beta filter without a monochromator. It was also analyzed with a Fourier Transform Infrared Spectrum Two (FT-IR) spectrometer (PerkinElmer, USA) equipped with a $LiTaO_3$ detector. The elemental composition and chemical states on the surface of precipitates were detected with an X-ray photoelectron spectrometer (XPS, Kratos Axis Ultra) with monochromated Al Kα-radiation using a pass energy of 40 eV, X-ray power of 150 W, charge neutralization, and analysis area of approximately 700 μm × 300 μm. The carbon 1 s peak at 284.8 eV was used as the binding energy reference. The elemental composition was determined from the peak areas of high-resolution core level spectra after Shirley background subtraction using equipment-specific sensitivity factors.

## 3. Results and discussion

In a hydrometallurgical recovery process, Fe and Al need to be removed prior to the solvent extraction of valuable metals (e.g., Ni, Co, and Mn) from LIB PLS; therefore, the typical route is to remove them by increasing the pH, i.e., hydrolysis. In the current study, we studied Fe and Al removal from industrial battery waste leach solution. Specifically, the focus was on the impact of typical impurities present in battery waste, i.e., phosphorus (phosphate), fluoride, and copper.

### 3.1. Fe and Al precipitation as a function of pH

When studying iron removal from industrial BM based PLS, the precipitation efficiency at 60 °C for Fe as well as for P was found to be high (97.8 % and 93.2 %, respectively), even at the lowest studied pH level (pH 2.0), Fig. 1. Additionally, it increased to > 99 % for Fe and > 96 % for P at pH 2.5–4.5. In contrast, the precipitation efficiency of Al at pH 2.0 was only 22.9 %. This result shows that, for an industrial BM-LFP based leach solution, desirable separation efficiency between Fe and Al can be achieved at pH 2.5, as high Fe precipitation was supported by the availability of $PO_4^{3-}$ ions (amorphous $FePO_4$, Fig. S1) but only minor contamination by aluminum occurred. The pH used in Fe removal in the current study differs clearly from earlier published findings (in $PO_4^{3-}$ deficient systems) where > 99 % Fe precipitation was achieved only at pHs > 3.5 (NaOH precipitation) (Chernyaev et al., 2023). However, the precipitation order was found to be similar (Beak et al., 2022) as Fe precipitated first (at ~ 3.0) and Al precipitated only after that (at pH 4.0–5.0) from the leaching PLS from BM with a lower Fe content (0.1–0.9 wt%). This was done by adding $H_3PO_4$ acid first followed by NaOH to adjust the solution pH at 20–95 °C.

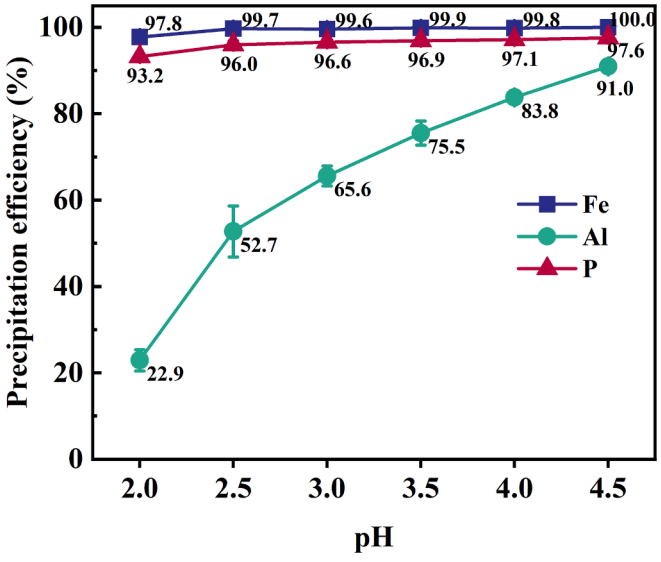


**Fig. 1.** Precipitation efficiency of Fe, Al, and P from industrial BM based PLS ($t$ = 3 h, $T$ = 60 °C, $\omega$ = 300 rpm).

As the solution pH value was raised from 2.0 to 4.5, the concentration of $PO_4^{3-}$ increased slightly, primarily attributed to the ionization of phosphoric acid. According to Table 4, the order of the solubility product constants for metal phosphates is $Li_3PO_4$ > $AlPO_4$ > $FePO_4$ > $Mn_3(PO_4)_2$ > $Ni_3(PO_4)_2$ > $Cu_3(PO_4)_2$, suggesting that $AlPO_4$ has greater solubility compared to the other metal phosphates under the same conditions in a pure system. However, in $Me^{n+}$-$PO_4^{3-}$–$H_2O$ system, Liang et al. (Liang et al., 2020) found that the order of precipitation at pH 1.0–4.8 produce phosphate precipitates in the following order: $Fe^{3+}$ > $A1^{3+}$ > $Cu^{2+}$≈ $Fe^{2+}$ > $Co^{2+}$> $Mn^{2+}$≈ $Ni^{2+}$ > $Li^{+}$. It should be noted that Al concentration (1.19 g/L) of the solution investigated in the current study lower than concentrations of other dissolved metal ions (Fe 18.04 g/L, Ni 12.72 g/L, Co 7.51 g/L, Mn 6.96 g/L, Li 5.90 g/L, Cu 2.09 g/L). Thus, the other metal ions have higher tendency to complex with $PO_4^{3-}$ than $Al^{3+}$. Additionally, the precipitation efficiency of P increased by 4.40 %-units from pH 2.0 to 4.5. Most likely 93.2 % of P (or phosphate) precipitated with Fe already at pH ≤ 2.0, while the remaining phosphate could potentially complex with Al. However, the Al precipitation efficiency increased by 68.10 %-units when pH was increased from 2.0 to 4.5. Therefore, this suggests that the majority of $PO_4^{3-}$ continues to react preferentially with iron ions–and potentially with other dissolved metal ions–rather than with aluminum ions, as there is no clear correlation between Al and P precipitation (Fig. 1). The precipitation efficiency of aluminum increases in tandem with the rise in pH, indicating that this precipitation reaction is driven by the increased concentration of hydroxyl ions ($OH^-$) rather than $PO_4^{3-}$. Therefore, aluminum removal can be suggested to occur via the formation of aluminum oxides or hydroxides, which is similar to the hydroxide precipitation tests from phosphorus-free PLS solution in a previous study (Chernyaev et al., 2023). It can be concluded that, although iron precipitation is significantly affected by the presence of $PO_4^{3-}$, there is negligible reactivity between $PO_4^{3-}$ and aluminum ions in the studied system.

At pH 4.5, the precipitation efficiencies of Fe, P, and Al were 100 %, 97.6 %, and 90.7 %, respectively, allowing almost full removal of the studied impurities. The standard deviations in the three repeated experiments for Fe, P, and Al were 0, 0.02, and 0.6 % units, respectively. Error margins at the studied pH values are presented in Fig. 1, but the deviations are so small that they can be seen only for Al. It is worth noting that iron and aluminum can form both hydroxides and phosphates at elevated pH (Speight and Lang, 2004). Based on calculation with HSC 10 Chemistry software (version 10.0.5.16, Metso Outotec) (Metso, 2024), $K_{sp}$ value at 60 °C for $FePO_4$ is $1.4\times10^{-27}$, whereas for aluminum ($AlPO_4$) it is $4.0\times10^{-20}$. When considering the investigated solution composition, the stoichiometric amount of P needed for both Fe (18 g/L in the PLS sample) and Al (1 g/L in the PLS sample) precipitation would be 11.3 g/L, whereas in the current study the P concentration was 11 g/L. This also indicates that, stoichiometrically, there would not be quite enough P to precipitate both Fe and Al as phosphates. Phosphate precipitation for both Fe and Al has also been suggested to be favored over hydroxide precipitation in a pH range of ~ 3 (Chernyaev et al., 2023).

### 3.2. Characterization of Fe and Al precipitates

Two precipitates obtained in Fe and Al removal at pH 2.0 (P1-1#) and pH 4.5 (P6-3#) were further analyzed by XPS (Fig. 2), and their atomic contents are listed in Table 5. However, the values mentioned differ from the EDS analysis result (Fig. S2 and S3) since XPS is a very surface-sensitive technique (analysis depth < 5 nm), and the content shown is present only at the tested surface spots of the samples.

The Fe 2p spectrum has two components: Fe $2p_{3/2}$ and Fe $2p_{1/2}$, due to spin–orbit coupling, each consisting of a main peak and two shake-up satellites, as shown in Fig. 2 (a) and (b). The binding energies for the Fe $2p_{3/2}$ and Fe $2p_{1/2}$ main peaks were centered at 712.4 eV and 725.5 eV in the pH 2.0 precipitate as well as 712.1 eV and 725.2 eV in the pH 4.5

**Table 4**
Solubility product constants for potential metal phosphates in the studied system at 25° C.

| phosphates | $FePO_4$ | $AlPO_4$ | $Cu_3(PO_4)_2$ | $Ni_3(PO_4)_2$ | $Co_3(PO_4)_2$ | $Mn_3(PO_4)_2$ | $Li_3PO_4$ |
|---|---|---|---|---|---|---|---|
| Ksp | $10^{-21.89}$ | $10^{-20.01}$ | $10^{-36.85}$ | $10^{-31.32}$ | $10^{-34.69}$ | $10^{-31.21}$ | $10^{-10.63}$ |

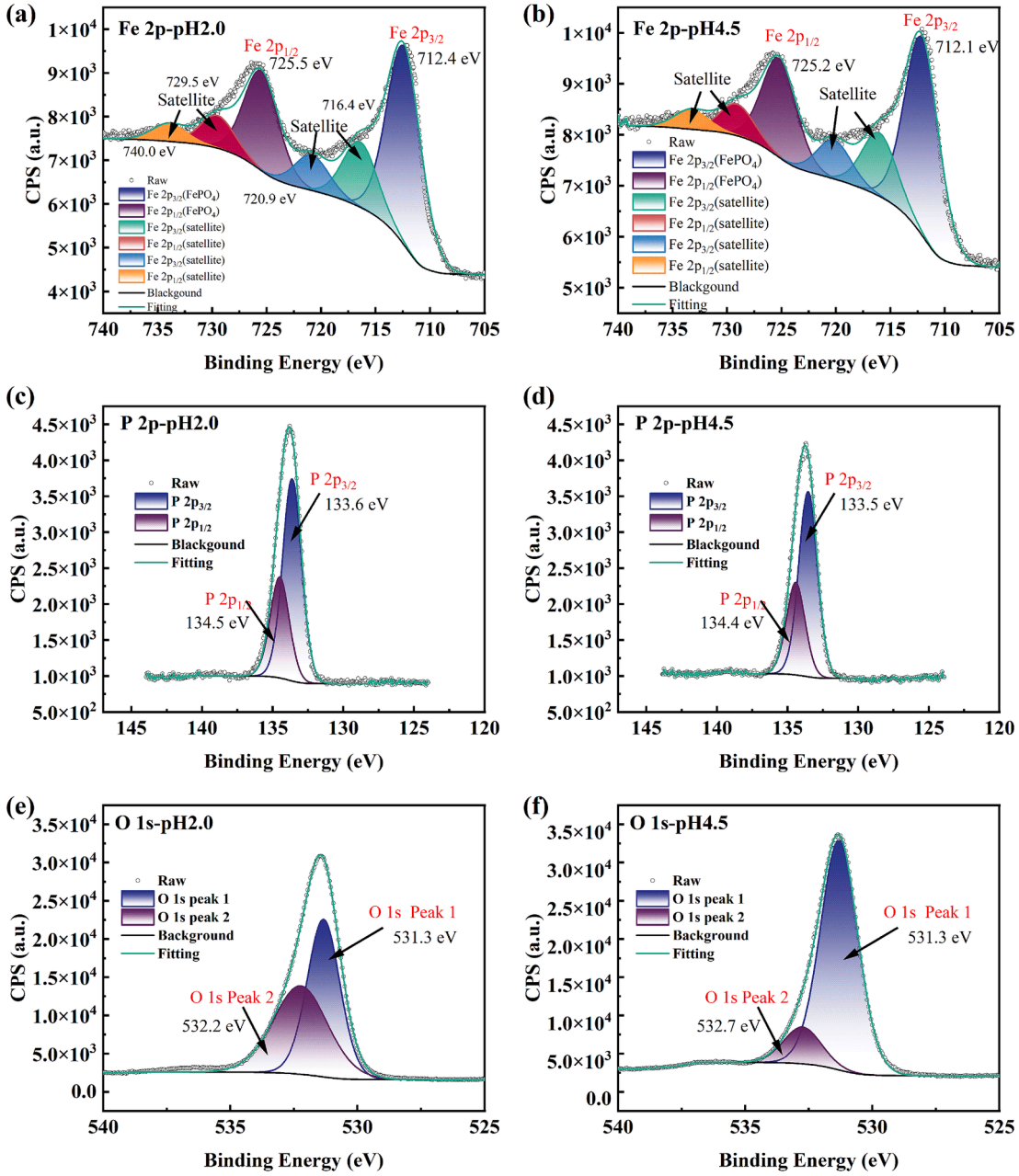


**Fig. 2.** X-ray photoelectron spectroscopy spectra of precipitate at pH 2.0 (P1-1#) and pH 4.5 (P6-3#). (a, b for Fe; c, d for P; e, f for O; g, h for Al, and i, k for F).

precipitate. The results indicate that the iron element in the precipitations existed in the form of $Fe^{3+}$ (Castro et al., 2010; Jie et al., 2021). The P 2p spectrum of the precipitates also displays the spin–orbit doublets of P $2p_{3/2}$ and P 2p 1/2 separated by 0.9 eV, with the P $2p_{3/2}$ component at 133.5–133.6 eV. The observation of only one P 2p doublet is associated with the presence of P-O in $PO_4^{3-}$, $HPO_4^{2-}$, or $H_2PO_4$; therefore, Fe is mostly a phosphate based on the combined results of the two above spectra (Fe and P) (Castro et al., 2010; Jie et al., 2021) and their atomic ratios (1.7−1.9). The O 1 s spectrum was fitted with two peaks (Fig. 2e and 2f), the stronger of which at 531.3 eV was related to the P-O in $PO_4^{3-}$ or $Al_2O_3$ (Chastain and King Jr., 1992), whereas the weaker one at 532.7 eV below pH 4.5 was associated with O–H as well as 532.2 eV at pH 2.0 related to the oxygen atom of the $SO_4^{2-}$ group. The characteristic peaks of Al 2p that appeared at 74.9 eV and 75.3–75.4 eV were related to Al-O (Tay et al., 2022), indicating that the Al element was in the form of aluminum oxide when combined the analysis of Section 3.1. The characteristic peak of F 1 s centered at 685.0 eV is ascribed to Fe-F (Jie et al., 2021). In summary, Fe precipitates predominantly as $FePO_4$ with a

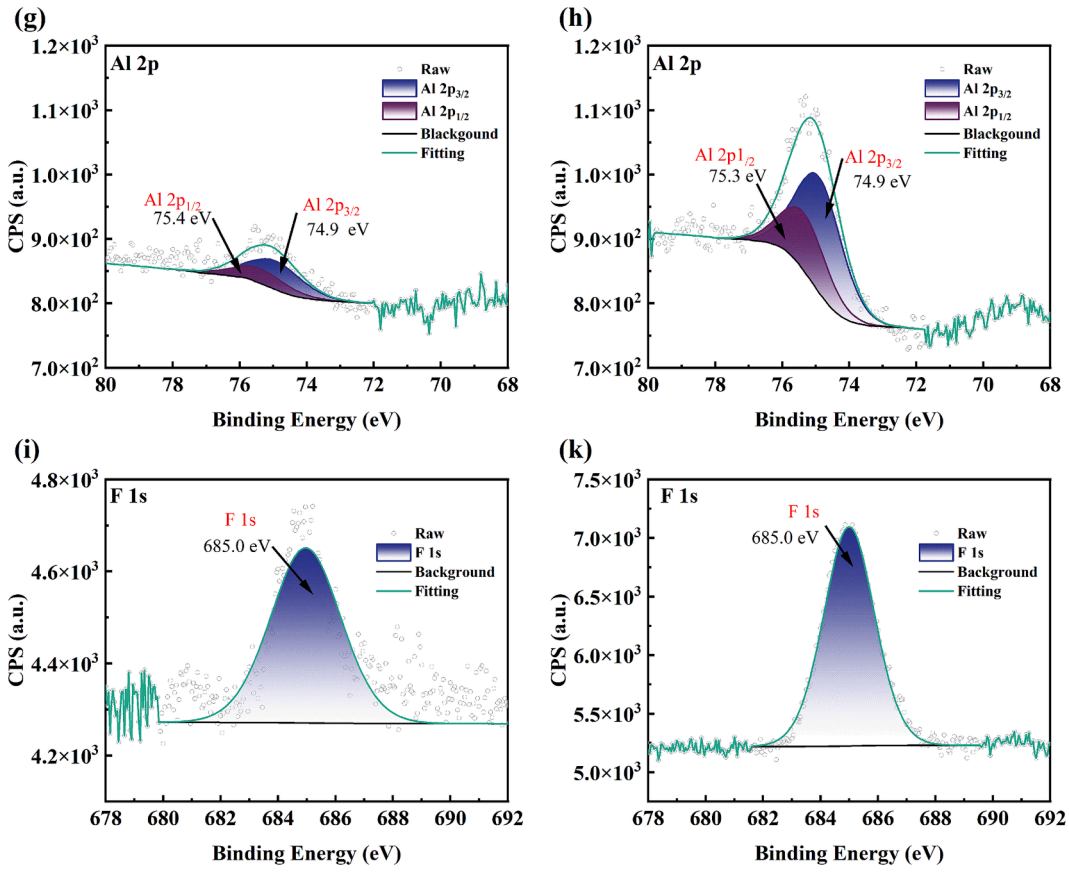


**Fig. 2.** (*continued*).

**Table 5**
Atomic contents (at.%) of precipitates analyzed by XPS.

| Precipitates | C | O | Fe | Al | P | S | F | Na | P/Fe | O/P | P/Al | O/Al |
|---|---|---|---|---|---|---|---|---|---|---|---|---|
| pH2.0 | 20.7 | 57.4 | 6.5 | 0.3 | 10.9 | 2.3 | 0.6 | 1.3 | 1.7 | 5.3 | 36.3 | 191.3 |
| pH4.5 | 19.5 | 56.3 | 4.9 | 2.0 | 9.2 | 1.9 | 2.7 | 3.5 | 1.9 | 6.1 | 4.6 | 28.2 |

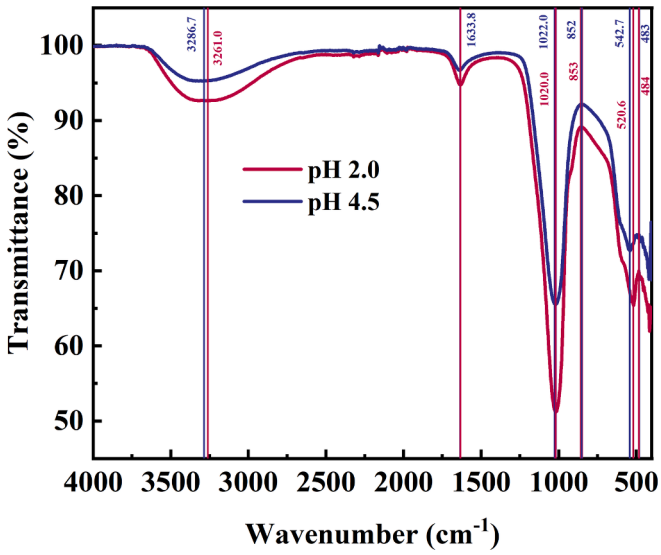


**Fig. 3.** FT-IR spectra of precipitates at pH 2.0 (P1-1#) and pH 4.5 (P6-3#).

minor fraction as $FeF_3$, while aluminum was found in the precipitate mainly as oxidized aluminum (AlOOH or $Al_2O_3{\cdot}H_2O$).

The two selected precipitates (at pH 2.0 and pH 4.5) were also analyzed by FTIR, Fig. 3. The bands around 1634 $cm^{-1}$ as well as the bands at approximately 3261–3286 $cm^{-1}$ of the two samples were ascribed to the O–H vibration of adsorbed water molecules, which may be from aluminum oxide (AlOOH or $Al_2O_3{\cdot}H_2O$). The two precipitates presented a slight difference in the FT-IR spectrum. The bands at 1020–1022 $cm^{-1}$ were ascribed to the symmetric $PO_4$- stretching mode associated with the $Q^0$ $PO_4^{3-}$ tetrahedral (Liu et al., 2017; Zhang and Brow, 2011). The peaks at around 536 $cm^{-1}$ (521 $cm^{-1}$ at pH 2.0 and 543 at pH 4.5) and 483–484 $cm^{-1}$ were also assigned to the symmetric stretching mode of the $SO_3$ group, while the peaks at 852–853 $cm^{-1}$ were related to the stretching of the S-OH group (Weng and Xu, 2016). As a result, we suggest that the precipitates mainly exist in the form of phosphate due to the high transmittance.

### 3.3. Behavior of F during Fe and Al precipitation

Approximately 85 % of the fluorine was effectively precipitated from the PLS along with iron and aluminum already at pH 2.0, Fig. 4. The F removal efficiency increased to 91.0 % as the pH was raised to 4.5, in line with findings from Jie et al., 2021 (Jie et al., 2021), and Ntuk et al.,

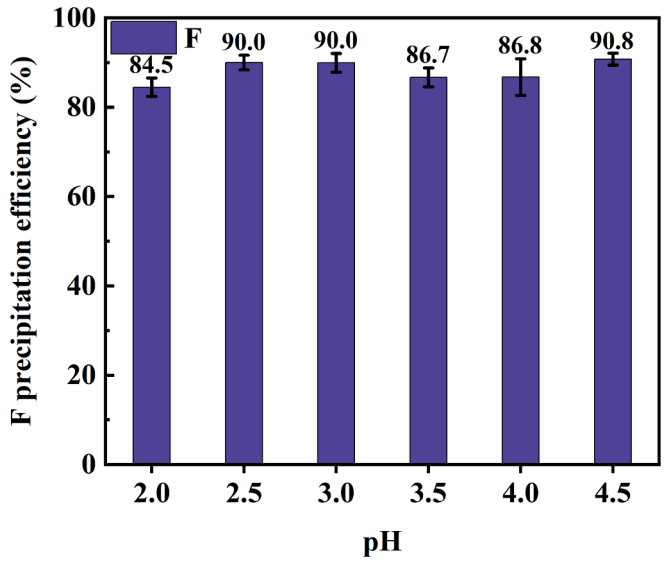


**Fig. 4.** F precipitation along with Fe and Al removal ($t$ = 3 h, $T$ = 60 °C, $\omega$ = 300 rpm).

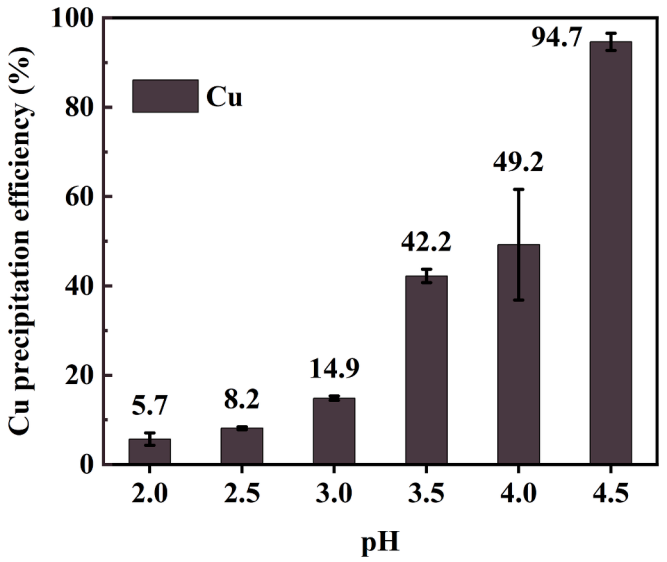


**Fig. 5.** Cu precipitation along with Fe and Al removal ($t$ = 3 h, $T$ = 60 °C, $\omega$ = 300 rpm).

2015 (Ntuk et al., 2015). Fluorine demonstrated the capability of precipitating with battery metals, generating compounds such as $AlF_3$, $FeF_3$, LiF, $CuF_2$, $MnF_2$, $NiF_2$, and $CoF_2$ (Speight and Lang, 2004). Throughout this study, iron exhibited consistently high precipitation efficiency, ranging from 97.8 % to 100 % across all investigated pH values, as depicted in Fig. 1.

In contrast, aluminum precipitation efficiency increased with rising pH, reaching 90.8 % at pH 4.5. This trend is consistent with the findings of Chernyaev et al. (Chernyaev et al., 2023), indicating that the presence of fluorine in the solution allows for the complete removal of iron via additional formation of $FeF_3$ phase, while the presence of fluoride does not support aluminum precipitation, as indicated by XPS analysis (Fig. 2). Instead, the resilience in aluminum precipitation is suggested to be attributed to the formation of robust Al-F complexes, including $AlF^{2+}$, $AlF_2^+$, $AlF_3$(aq), $AlF_3OH^-$, $AlF_4^-$, $AlF_5^{2-}$, and $AlF_6^{3-}$. It is also possible that F (originating from BM leaching, $LiPF_6$) can complex aluminum as soluble complexes (Al-F complexes), thereby keeping the prevailing species of aluminum in dissolved form (Fig. 1). Additionally, precipitated aluminum (AlOOH or $Al_2O_3{\cdot}H_2O$) can have a strong adsorption property (Adeno et al., 2014), which may cause increased metal losses with increased Al precipitation.

### 3.4. Behavior of copper during Fe and Al precipitation

Copper is a typical metal in BM, originating from the anode current collectors of LIBs. Copper can be technically removed from hydrometallurgical battery recycling solutions already prior to Fe and Al removal via cementation or alternative methods (Peng et al., 2019; Virolainen et al., 2021; Wang and Friedrich, 2015). However, it is also possible that no separate removal step is conducted, and, instead, copper is removed together with Fe and Al via hydrolysis with increasing pH values. For example, Klaehn et al. (Klaehn et al., 2023) found that 78.9 % of copper is precipitated at pH 3.8 with only diammonium hydrogen phosphate (DAP), whereas 53.6 % was removed at pH 4.0 with a combination of DAP and ammonium hydroxide ($NH_4OH$) due to the complex between Cu and $NH_4^+$ as well as $NH_3$.

In the current study, copper cementation was not conducted; therefore, the PLS also contained 2.1 g/L dissolved copper originating from industrial battery waste. The precipitation efficiency of copper is similar to that of aluminum and increases in tandem with a pH increase, suggested to be driven by the increased concentration of hydroxyl ions ($OH^-$) rather than $PO_4^{3-}$. At pH levels below 3.0, the removal of $Cu^{2+}$ was < 15 %, see Fig. 5. At this pH, iron was almost fully precipitated with $PO_4^{3-}$, further highlighting the selectivity for iron removal (vs. other metals). Within the pH range of 3.5 to 4.0, copper precipitation increased significantly to 42–49 %. This was attributed to the interaction of $Cu^{2+}$ not only with $PO_4^{3-}$, but also with $OH^-$. Upon reaching a pH value of 4.5, approximately 95 % of the $Cu^{2+}$ was precipitated. This is similar to the results of the study by Wang et al. (Wang and Friedrich, 2015), where copper was precipitated predominantly through its reaction with $OH^-$ to form $Cu(OH)_2$. This shows that almost complete precipitation of Fe and Al from the studied solution would also result in almost total copper removal.

### 3.5. Losses of battery cathode materials (Li, Ni, Co, and Mn) along with Fe and Al removal

It has been found earlier that the co-precipitation efficiencies of valuable battery metals in the presence of phosphates can be lower when compared to hydroxide precipitation (Chernyaev et al., 2023). Chernyaev et al. found that the co-precipitation of NMC metals and lithium was less than 1 % at pH 3.0, and about 1 % in the presence of phosphates at pH 4.0 (Chernyaev et al., 2023). In the absence of phosphates in hydroxide precipitation, the corresponding values at pH 3.0 were less than 1 %, whereas they varied between 1 % and 5 % at pH 4.0. These findings were related to synthetic solutions and not the real BM based PLS. Therefore, this is addressed in the current study by the use of industrial BM based PLS.

Fig. 6 depicts the co-precipitation for Li, Ni, Co, and Mn in the conditions of the current study. The co-precipitation efficiencies for the above metals were found to increase with increasing pHs. Specifically, Li co-precipitation increased from 4.4 % at pH 2.0 to 9.2 % at pH 4.5, whereas for Ni, it increased from 4.8 % (pH 2.0) to 12.7 % (pH 4.5). Co showed a greater increase, from 4.5 % at pH 2.0 to 17.3 % at pH 4.5. Mn exhibited the most significant increase, with a co-precipitation tendency of 4.8 % at pH 2.0 and 26.4 % at pH 4.5. All these values are substantially higher when compared to the synthetic solutions without P of the previous study (2.0 % Ni, 2.2 % Co, and 0.3 % Li at pH 4.25 via phosphate precipitation) (Chernyaev et al., 2023). It can be assumed that the large difference in phosphorus content in the PLS (30 times) may have led to this major discrepancy. In fact, all major battery metals such as Li, Ni, Co, and Mn can react with phosphate to form precipitates.

It is hypothesized that the Al oxide hydroxide gel (AlOOH or $Al_2O_3{\cdot}H_2O$ based on the XPS results) formed in the current study may

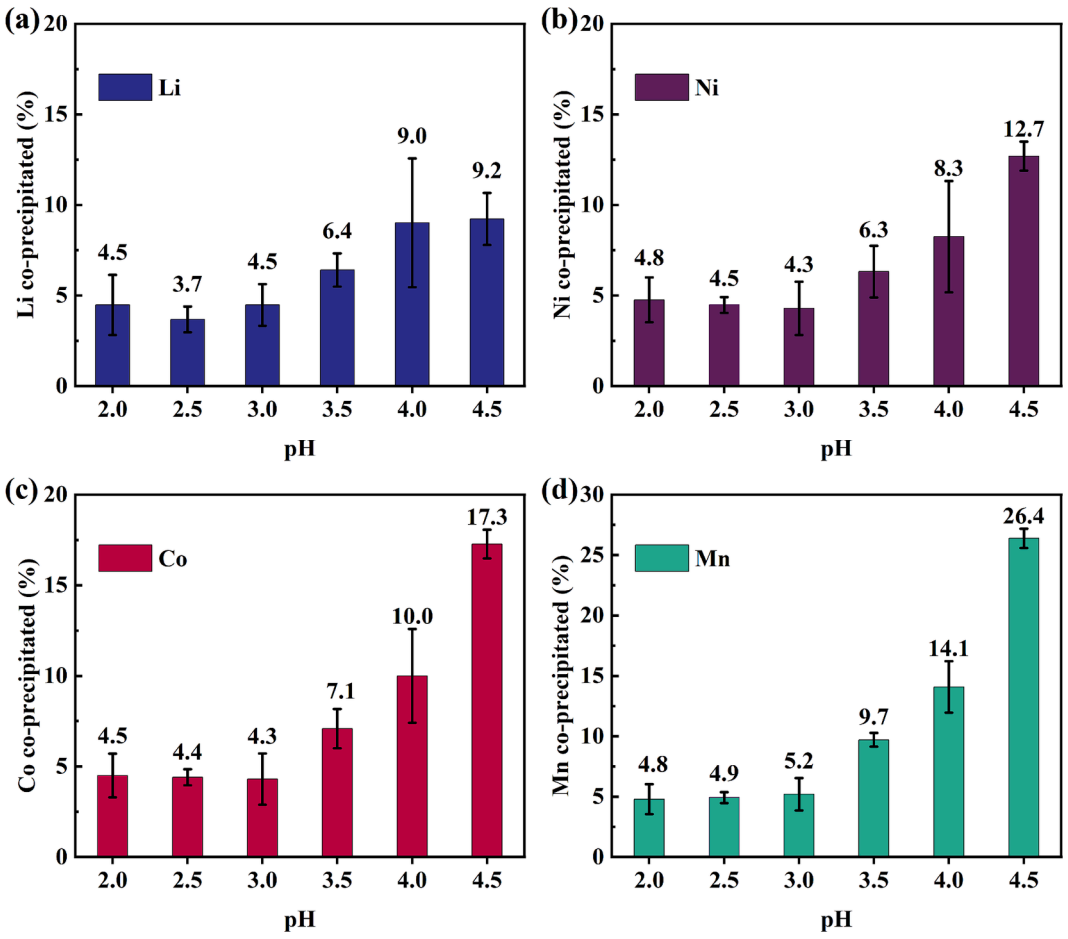


**Fig. 6.** Co-precipitation (%) of (a) Li; (b) Ni; (c) Co; (d) Mn ($t$ = 3 h, $T$ = 60 °C, $\omega$ = 300 rpm).

also adsorb NMC metals and lithium, thus causing a higher risk of co-precipitation and losses of valuable metals. Furthermore, the absence of copper removal may impact on the precipitation behavior as co-precipitation of copper may also initiate earlier co-precipitation of other valuable battery elements. In addition, the results of this study are similar to those of Wang and Friedrich (Wang and Friedrich, 2015), who recommended a pH range of 3.5–4.0 for sufficient Fe and Al removal, with Co, Ni, and Mn losses averaging between 3 % and 5 %. However, the losses of Co, Ni, and Mn in the current study were higher when compared to the results of Wang and Friedrich (Wang and Friedrich, 2015).

The results here suggest that it may be hard to avoid co-precipitation of NMC metals and Li when conducting neutralization and solution purification for PLS rich in phosphorus. The co-precipitation tendency of valuable metals seems clear at all pH values, even at pH 2.0 where iron phosphate precipitation dominates. This suggests that even though iron phosphate precipitation seems to result in NMC metal losses, the formation of Co or Ni hydroxides may have begun at higher pH due to the high co-precipitation tendency in the current system.

### 3.6. Precipitation strategies

Based on the results of the current study, it can be suggested that the impurity (Fe, Al) separation process can be carried out using either *combined* or *selective* removal of Fe and Al, Fig. 7. If the *combined process* is used, the pH is directly increased to pH 4.5. In experiments P6-1#, 2#, and 3# using the *combined process*, amorphous $FePO_4$ as well as aluminum hydroxides may have formed with strong adsorption properties (Naeem et al., 2007), and they can easily cause Ni, Co, and Mn losses via physical or chemical adsorption. Furthermore, already at pH 4.5, some hydrolysis of these dissolved metals may also have occurred. In the current study (P6-1#, 2#, and 3#), the pH 4.5 purified solution contained ca. 11.7 g/L Ni, 6.7 g/L Co, 5.2 g/L Mn, 3.9 g/L Li, 0.3 g/L P, 0.2 g/L F, 0.1 g/L Cu, 0.1 g/L Al, and 0.0 g/L Fe. The purified PLS is suitable for further state-of-the-art battery metals processing, notwithstanding notable losses of Li, Ni, Mn, and Co (9.2 %, 12.7 %, 26.4 % and 17.3 %, respectively). A more concentrated solution could be achieved by using a higher S/L ratio (e.g., 156.5 g/L) in leaching; however, the percentual losses of valuable metals are expected to remain at a similar level. The solid precipitate had a composition of 18.4 wt% Fe, 11.4 wt% P, 2.0 wt% Cu, 1.9 wt% Mn, 1.6 wt% Ni, 1.3 wt% Co, 1.1 wt% Al, 0.6 wt % Li, and 0.2 wt% F.

Compared with *combined process* precipitation, a *selective process* may be more favorable for the reduction of battery metal losses. In a *selective process*, Fe is first removed through phosphate precipitation as $FePO_4$ at ~ pH 2.0. Here, the losses of nickel, cobalt, and manganese are expected to be lower since $FePO_4$ adsorption in acidic solution is relatively weaker and nickel, cobalt, and manganese do not form hydroxide precipitates at pH 2. In this study, Li, Ni, Mn, and Co losses at pH 2 were 4.5 %, 4.8 %, 4.8 %, and 4.5 %, respectively. When Fe was removed, the purified PLS contained 16.8 g/L Ni, 10.0 g/L Co, 7.9 g/L Mn, 5.0 g/L Li, 2.8 g/L Cu, 1.3 g/L Al, 1.00 g/L P, 0.5 g/L Fe, and 0.3 g/L F. The solid precipitate of this unit process was iron- and phosphate-rich (21.5 wt% Fe and 13.4 wt % P) while minor co-precipitation of battery metals was observed as well (0.7 wt% Ni, 0.4 wt% Mn, 0.4 wt% Co, 0.4 wt% Al, 0.3 wt% Li, 0.1 wt% Cu, and 0.1 wt% F). This kind of precipitate may act as a potential intermediate for further iron phosphate purification and valorization, improving the circular economy of the currently overlooked iron-rich

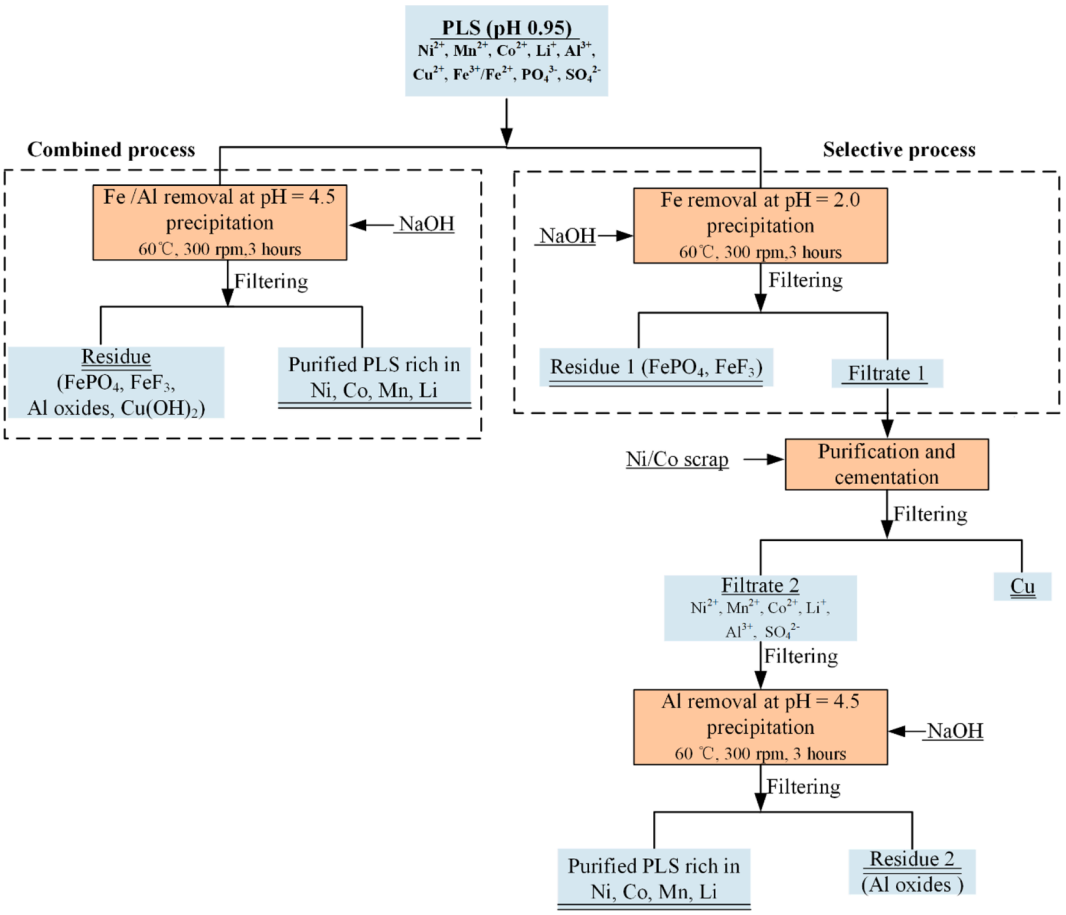


**Fig. 7.** Suggested block diagram of Fe and Al removal for hydrometallurgical NMC-LFP recycling process (dashed line marks the experimental focus of the current study).

impurity fractions of battery recycling processes.

In the *selective process*, the Fe-free solution needs to be subjected to additional solution purification steps in order to remove Al and copper. Copper cementation could be conducted using Al powder for instance, although Al may passivate (Shukla et al., 2023) and cause increasing challenges due to amorphous gel-like precipitates in the precipitation stage. Therefore, metallic Co or Ni or scrap alloy would be preferred materials for use in copper cementation. Alternatively, Cu may be removed together with Al at pH 4.5 by NaOH addition (*combined process*). When the Fe-free filtrate is adjusted to pH 4.5, aluminum is precipitated, resulting in purified Ni-Mn-Co-Li solution for state-of-the-art battery metals recovery. There are also battery metal losses in such an Fe-free system (in the absence of $FePO_4$ precipitate) but it can be hypothesized that the losses would be lower. If 4.5–4.8 % losses are estimated for Li, Ni, Mn, and Co, the purified PLS would contain 5.0 g/L Li, 16.8 g/L Ni, 7.9 g/L Mn, 10.0 g/L Co and very low concentrations of Cu, P, and F. The actual losses in Fe-free Al precipitation are not experimentally defined in the current study, and therefore the losses in the *selective process* along with the pH increase are only estimates.

## 4. Conclusion

This study highlights the precipitation efficiency of iron and aluminum from industrial NMC battery waste recycling solution, in the presence of elevated iron and phosphorus concentrations, originating from the synergistic recycling of LFP. High metal removal efficiencies for both Fe and Al can be achieved at pH 4.5 (100 % of Fe, 91.0 % of Al) with simultaneous precipitation of phosphorus, copper, and fluoride (97.6 % of P, 94.7 % of Cu, and 90.8 % of F). However, this precipitation is associated with relatively high losses of Li (9.2 %), Ni (12.7 %), Co (17.3 %), and Mn (26.4 %) via co-precipitation. In more acidic solutions, selective precipitation for iron can be achieved already at pH = 2.0 with 97.8 % efficiency. In such a process there is good selectivity vs. aluminum, i.e., only 22.9 % of aluminum is co-precipitated. This shows the efficiency of $PO_4^{3-}$ ions to precipitate $Fe^{3+}$ already at lower pH values, while a minor amount of $FeF_3$ is also formed. The presence of phosphate ions may also cause minor co-precipitation of battery metals (Ni, Li, Co, and Mn, of 4.8 %, 4.5 %, 4.5 %, and 4.8 %, respectively) already at pH 2.0. Surprisingly, Al was found not to precipitate with phosphates; instead, it may form complexes with fluoride ($AlF^{2+}$, $AlF_2^+$, $AlF_3$(aq), $AlF_3OH^-$, $AlF_4^-$, $AlF_5^{2-}$, and $AlF_6^{3-}$) and hydrolyze (e.g., as AlOOH) only with increased pH (91.0 % at pH = 4.5). This study not only demonstrated the precipitation phenomena and dominant phases during iron and aluminum removal from industrial battery waste PLS, but also emphasized the strategic considerations required for optimizing the recovery of valuable battery metals in the recycling process.

## CRediT authorship contribution statement

**Yuanmin Zou:** Writing – review & editing, Writing – original draft, Visualization, Validation, Methodology, Investigation, Formal analysis, Data curation, Conceptualization. **Alexander Chernyaev:** Writing – review & editing, Validation, Methodology. **Sipi Seisko:** Writing – review & editing, Project administration. **Jani Sainio:** Writing – review & editing, Data curation. **Mari Lundström:** Writing – review & editing, Supervision, Project administration, Funding acquisition, Conceptualization.

## Declaration of competing interest

The authors declare that they have no known competing financial interests or personal relationships that could have appeared to influence the work reported in this paper.

## Data availability

Data will be made available on request.

## Acknowledgements

This study has been funded by the BATCircle2.0 project (Business Finland grant number 44886/31/2020). Additionally, the RawMatTERS Finland Infrastructure (RAMI), supported by the Academy of Finland, is gratefully acknowledged.

## Appendix A. Supplementary data

Supplementary data to this article can be found online at https://doi.org/10.1016/j.mineng.2024.109037.

## References

Adeno, F., Mulugeta, E., Zewge, F., Chebude, Y., 2014. Adsorptive removal of fluoride from water using nanoscale aluminium oxide hydroxide (AlOOH). Bull. Chem. Soc. Ethiop. 28, 215–227. https://doi.org/10.4314/bcse.v28i2.6.

Agarwal, V., Khalid, M.K., Porvali, A., Wilson, B.P., Lundström, M., 2019. Recycling of spent NiMH batteries: Integration of battery leach solution into primary Ni production using solvent extraction. SM&T. 22, e00121.

Beak, M., Park, J., Park, S., Jeong, S., Kang, J., Choi, W., Yoon, W.-S., Kwon, K., 2022. Understanding the effect of nonmetallic impurities in regenerated cathode materials for lithium-ion battery recycling by tracking down impurity elements. J. Hazard. Mater. 425, 127907. https://doi.org/10.1016/j.jhazmat.2021.127907.

Castro, L., Dedryvère, R., El Khalifi, M., Lippens, P.-E., Bréger, J., Tessier, C., Gonbeau, D., 2010. The spin-polarized electronic structure of $LiFePO_4$ and $FePO_4$ evidenced by in-lab XPS. J. Phys. Chem. C 114, 17995–18000. https://doi.org/10.1021/jp106631v.

Chastain, J., King Jr, R.C., 1992. Handbook of X-ray photoelectron spectroscopy. Perkin-Elmer Corporation.

Chen, W.-S., Ho, H.-J., 2018. Recovery of valuable metals from lithium-ion batteries NMC cathode waste materials by hydrometallurgical methods. Metals 8, 321. https://doi.org/10.3390/met8050321.

Chernyaev, A., Zhang, J., Seisko, S., Louhi-Kultanen, M., Lundström, M., 2023. $Fe^{3+}$ and $Al^{3+}$ removal by phosphate and hydroxide precipitation from synthetic NMC Li-ion battery leach solution. Sci. Rep. 13, 21445. https://doi.org/10.1038/s41598-023-48247-6.

Cordell, D., Drangert, J.-O., White, S., 2009. The story of phosphorus: Global food security and food for thought. Glob. Environ. Change, Traditional Peoples and Climate Change 19, 292–305. https://doi.org/10.1016/j.gloenvcha.2008.10.009.

Daneshgar, S., Callegari, A., Capodaglio, A.G., Vaccari, D., 2018. The potential phosphorus crisis: resource conservation and possible escape technologies: a review. Resources 7, 37. https://doi.org/10.3390/resources7020037.

Dobó, Z., Dinh, T., Kulcsár, T., 2023. A review on recycling of spent lithium-ion batteries. Energy Rep. 9, 6362–6395. https://doi.org/10.1016/j.egyr.2023.05.264.

European Commission, 2017. 2017 List of Critical Raw Materials for the EU. https://eur-lex.europa.eu/legal-content/EN/TXT/PDF/?uri=CELEX:52017DC0490.

European Commission, 2023. Regulation of the European parliament and of the Council concerning batteries and waste batteries, amending Directive 2008/98/EC and Regulation (EU) 2019/1020 and repealing Directive 2006/66/EC. https://data.consilium.europa.eu/doc/document/PE-2-2023-INIT/en/pdf.

Guan, J., Li, Y., Guo, Y., Su, R., Gao, G., Song, H., Yuan, H., Liang, B., Guo, Z., 2017. Mechanochemical process enhanced cobalt and lithium recycling from wasted lithium-ion batteries. ACS Sustain. Chem. Eng. 5, 1026–1032. https://doi.org/10.1021/acssuschemeng.6b02337.

Guzolu, J.S., Gharabaghi, M., Mobin, M., Alilo, H., 2017. Extraction of Li and Co from Li-ion batteries by chemical methods. J. Inst. Eng. India Ser. D 98, 43–48. https://doi.org/10.1007/s40033-016-0114-z.

Hu, C., Guo, J., Wen, J., Peng, Y., 2013. Preparation and electrochemical performance of nano-$Co_3O_4$ anode materials from spent Li-ion batteries for lithium-ion batteries. J. Mater. Sci. Technol. 29, 215–220. https://doi.org/10.1016/j.jmst.2013.01.009.

Jantunen, N., Virolainen, S., Sainio, T., 2022. Direct production of Ni–Co–Mn mixtures for cathode precursors from cobalt-rich lithium-ion battery leachates by solvent extraction. Metals 12, 1445. https://doi.org/10.3390/met12091445.

Jiang, Y., Chen, X., Yan, S., Li, S., Zhou, T., 2021. Pursuing green and efficient process towards recycling of different metals from spent lithium-ion batteries through Ferro-chemistry. Chem. Eng. J. 426, 131637. https://doi.org/10.1016/j.cej.2021.131637.

Jie, Y., Yang, S., Shi, P., Chang, D., Fang, G., Mo, C., Ding, J., Liu, Z., Lai, Y., Chen, Y., 2021. Thermodynamic analysis and experimental investigation of Al and F removal from sulfuric acid leachate of spent $LiFePO_4$ battery powder. Metals 11, 1641. https://doi.org/10.3390/met11101641.

Johnston, A.E., Steen, I., 2002. Understanding phosphorus and its use in agriculture [WWW Document]. URL https://repository.rothamsted.ac.uk/item/88q94/understanding-phosphorus-and-its-use-in-agriculture (accessed 1.22.24).

Kang, J., Senanayake, G., Sohn, J., Shin, S.M., 2010. Recovery of cobalt sulfate from spent lithium-ion batteries by reductive leaching and solvent extraction with Cyanex 272. Hydrometall. 100, 168–171. https://doi.org/10.1016/j.hydromet.2009.10.010.

Klaehn, J.R., Shi, M., Diaz, L.A., Molina, D.E., Reich, S.M., Palasyuk, O., Repukaiti, R., Lister, T.E., 2023. Removal of impurity metals as phosphates from lithium-ion battery leachates. Hydrometall. 217, 106041. https://doi.org/10.1016/j.hydromet.2023.106041.

Kotrlý, S., Šůcha, L., 1985. Handbook of chemical equilibria in analytical chemistry. Ellis Horwood, Chichester.

Liang, H., Wang, D., Yang, S., Liu, Z., Cao, H., Rao, S., Zhang, K., 2020. Thermodynamics analysis and application on removal of aluminum in lixivium of spent ternary lithium-ion battery by phosphate precipitation. Nonferrous Metals (extractive Metallurgy in Chinese) 36–41.

Liu, Y., Li, Z., You, Y., Zheng, X., Wen, J., 2017. Synthesis of different structured $FePO_4$ for the enhanced conversion of methyl cellulose to 5-hydroxymethylfurfural. RSC Adv. 7, 51281–51289. https://doi.org/10.1039/C7RA09186A.

Lombardo, G., Ebin, B., St, J., Foreman, M.R., Steenari, B.-M., Petranikova, M., 2019. Chemical transformations in Li-Ion battery electrode materials by carbothermic reduction. ACS Sustain. Chem. Eng. 7, 13668–13679. https://doi.org/10.1021/acssuschemeng.8b06540.

Lv, W., Wang, Z., Cao, H., Sun, Y., Zhang, Y., Sun, Z., 2018. A critical review and analysis on the recycling of spent lithium-ion batteries. ACS Sustain. Chem. Eng. 6, 1504–1521. https://doi.org/10.1021/acssuschemeng.7b03811.

Makuza, B., Tian, Q., Guo, X., Chattopadhyay, K., Yu, D., 2021. Pyrometallurgical options for recycling spent lithium-ion batteries: A comprehensive review. J. Power Sources 491, 229622. https://doi.org/10.1016/j.jpowsour.2021.229622.

Martell, A.E., Smith, R.M., 1976. Critical Stability Constants Volume 4: Inorganic Complexes. Plenum Press, New York.

Metso, 2024. HSC Chemistry [WWW Document]. URL https://www.metso.com/portfolio/hsc-chemistry/ (accessed 3.29.24).

Naeem, A., Mustafa, S., Dilara, B., Ilyas, M., Samad, H.Y., Safdar, M., 2007. Sorption of isosteric heat of metal ions by $FePO_4$. J. Chem. Soc. Pak. 29, 1–4.

Ntuk, U., Tait, S., White, E.T., Steel, K.M., 2015. The precipitation and solubility of aluminium hydroxyfluoride hydrate between 30 and 70 °C. Hydrometall. 155, 79–87. https://doi.org/10.1016/j.hydromet.2015.04.010.

Partinen, J., Halli, P., Helin, S., Wilson, B.P., Lundström, M., 2022. Utilizing $Cu^+$ as catalyst in reductive leaching of lithium-ion battery cathode materials in $H_2SO_4$–NaCl solutions. Hydrometall. 208, 105808. https://doi.org/10.1016/j.hydromet.2021.105808.

Paulino, J.F., Busnardo, N.G., Afonso, J.C., 2008. Recovery of valuable elements from spent Li-batteries. J. Hazard. Mater. 150, 843–849. https://doi.org/10.1016/j.jhazmat.2007.10.048.

Peng, C., Chang, C., Wang, Z., Wilson, B.P., Liu, F., Lundström, M., 2020. Recovery of high-purity $MnO_2$ from the acid leaching solution of spent Li-ion batteries. JOM 72, 790–799. https://doi.org/10.1007/s11837-019-03785-1.

Peng, F., Mu, D., Li, R., Liu, Y., Ji, Y., Dai, C., Ding, F., 2019. Impurity removal with highly selective and efficient methods and the recycling of transition metals from spent lithium-ion batteries. RSC Adv. 9, 21922–21930. https://doi.org/10.1039/C9RA02331C.

Porvali, A., Aaltonen, M., Ojanen, S., Velazquez-Martinez, O., Eronen, E., Liu, F., Wilson, B.P., Serna-Guerrero, R., Lundström, M., 2019. Mechanical and hydrometallurgical processes in HCl media for the recycling of valuable metals from Li-ion battery waste. Resour. Conserv. Recycl. 142, 257–266. https://doi.org/10.1016/j.resconrec.2018.11.023.

Pranolo, Y., Zhang, W., Cheng, C.Y., 2010. Recovery of metals from spent lithium-ion battery leach solutions with a mixed solvent extractant system. Hydrometall. 102, 37–42. https://doi.org/10.1016/j.hydromet.2010.01.007.

Rinne, M., Elomaa, H., Porvali, A., Lundström, M., 2021. Simulation-based life cycle assessment for hydrometallurgical recycling of mixed LIB and NiMH waste. Resour. Conserv. Recycl. 170, 105586. https://doi.org/10.1016/j.resconrec.2021.105586.

Scheunis, L., Callebaut, W., 2023. Process for the recovery of lithium. CA3119203C.

Shin, S.M., Kim, N.H., Sohn, J.S., Yang, D.H., Kim, Y.H., 2005. Development of a metal recovery process from Li-ion battery wastes. Hydrometall. 79, 172–181. https://doi.org/10.1016/j.hydromet.2005.06.004.

Shukla, S., Chernyaev, A., Halli, P., Aromaa, J., Lundström, M., 2023. Leaching of waste pharmaceutical blister package aluminium in sulphuric acid media. Metals 13, 1118. https://doi.org/10.3390/met13061118.

Song, X., Hu, T., Liang, C., Long, H., Zhou, L., Song, W., You, L.S., Wu, Z.W., Liu, J., 2017. Direct regeneration of cathode materials from spent lithium iron phosphate batteries using a solid phase sintering method. RSC Adv. 7, 4783–4790. https://doi.org/10.1039/C6RA27210J.

Speight, J.G., Lang, N.A., 2004. Lange's handbook of chemistry, Sixteenth ed. McGraw-Hill.

Sun, Z., Cao, H., Xiao, Y., Sietsma, J., Jin, W., Agterhuis, H., Yang, Y., 2017. Toward sustainability for recovery of critical metals from electronic waste: the hydrochemistry processes. ACS Sustain. Chem. Eng. 5, 21–40. https://doi.org/10.1021/acssuschemeng.6b00841.

Takacova, Z., Havlik, T., Kukurugya, F., Orac, D., 2016. Cobalt and lithium recovery from active mass of spent Li-ion batteries: Theoretical and experimental approach. Hydrometall. 163, 9–17. https://doi.org/10.1016/j.hydromet.2016.03.007.

Tay, Y.S., Phua, E.J.R., Chen, Z., Gan, C.L., 2022. Simultaneous enhancement of polymerization kinetics and properties of phthalonitrile using alumina fillers. ACS Omega 7, 32996–33003. https://doi.org/10.1021/acsomega.2c02667.

Velázquez-Martínez, V., Santasalo-Aarnio, R., Serna-Guerrero, 2019. A critical review of lithium-ion battery recycling processes from a circular economy perspective. Batteries 5, 68. https://doi.org/10.3390/batteries5040068.

Virolainen, S., Wesselborg, T., Kaukinen, A., Sainio, T., 2021. Removal of iron, aluminium, manganese and copper from leach solutions of lithium-ion battery waste using ion exchange. Hydrometall. 202, 105602. https://doi.org/10.1016/j.hydromet.2021.105602.

Wang, H., Friedrich, B., 2015. Development of a highly efficient hydrometallurgical recycling process for automotive li-ion batteries. J. Sustain. Metall. 1, 168–178. https://doi.org/10.1007/s40831-015-0016-6.

Weng, S., Xu, Y., 2016. Fourier Transform Infrared Spectroscopy, FT-IR, The third edition. ed. Chemical Industry Press Co. Ltd.(CIP), Bejing.

Wesselborg, T., Virolainen, S., Sainio, T., 2021. Recovery of lithium from leach solutions of battery waste using direct solvent extraction with TBP and $FeCl_3$. Hydrometall. 202, 105593. https://doi.org/10.1016/j.hydromet.2021.105593.

Yuliusman, F.R., Nurqomariah, A., Silvia, 2018. Acid leaching and kinetics study of cobalt recovery from spent lithium-ion batteries with nitric acid. E3S Web Conf. 67, 03025. https://doi.org/10.1051/e3sconf/20186703025.

Zhang, L., Brow, R.K., 2011. A raman study of iron-phosphate crystalline compounds and glasses. J. Am. Ceram. Soc. 94, 3123–3130. https://doi.org/10.1111/j.1551-2916.2011.04486.x.

Zhang, K., Liang, H., Zhong, X., Cao, H., Wang, R., Liu, Z., 2022. Recovery of metals from sulfate leach solutions of spent ternary lithium-ion batteries by precipitation with phosphate and solvent extraction with P507. Hydrometall. 210, 105861. https://doi.org/10.1016/j.hydromet.2022.105861.

Zou, Y., Chernyaev, A., Ossama, M., Seisko, S., Lundström, M., 2024. Leaching of NMC industrial black mass in the presence of LFP. Sci. Rep. 14, 10818. https://doi.org/10.1038/s41598-024-61569-3.